Scripta Materialia 271 (2026) 116973

Contents lists available at ScienceDirect

Scripta Materialia

journal homepage: www.journals.elsevier.com/scripta-materialia

Unit-level hardening-driven strengthening in gradient nanotwinned Cu

Linhai Liu [a,b], Che Liu [a,b], Jin Zheng [a,b], Zhao Cheng [a,*], Lei Lu [a,1,*]

[a] Shenyang National Laboratory for Materials Science, Institute of Metal Research, Chinese Academy of Sciences, Shenyang 110016, China
[b] School of Materials Science and Engineering, University of Science and Technology of China, Shenyang 110016, China

ARTICLE INFO

Keywords:
Gradient nanotwinned Cu
Unit-level work hardening
Extra strengthening
Gradient plastic deformation
Geometrically necessary dislocations

ABSTRACT

Gradient nanotwinned (GNT) structures are a representative class of heterogeneous architectures that enhance the strength of metallic materials by introducing structural gradients. In this study, we show that both extra strengthening and work hardening in GNT Cu can be further improved by increasing the work hardening capacity of individual units, even with a constant structural gradient. Higher unit-level work hardening suppresses strain localization, facilitates more uniform gradient plastic deformation, and promotes the additional storage of geometrically necessary dislocations (GNDs) in formation of bundles of concentrated dislocations. These GNDs contribute significantly to the enhanced strengthening and hardening behavior of GNT Cu.

Gradient nanostructures (GNS) have emerged as a promising strategy for enhancing the mechanical performance of metallic materials, enabling the simultaneous improvement of strength, ductility, fatigue resistance and fracture toughness [1,2]. There have been extensive reports demonstrating that the gradient architectures incorporating with nanostructured units can overcome the conventional strength-ductility trade-off commonly observed in conventional homogeneous materials [3–7]. The superior performance of GNS metals is primarily attributed to gradient plastic deformation, which induces the storage of geometrically necessary dislocations (GNDs) [8–12]. These GNDs contribute to both strengthening and work hardening via kinematic and/or isotropic hardening mechanisms [13–15]. The extent of this strengthening/hardening effect is highly sensitive to the architectural parameters of the gradient structure.

Among various GNS architectures, gradient nanotwinned (GNT) structures offer a unique model system due to their precisely controllable gradients, as well as their well-characterized dislocation mechanisms in nanotwinned domains [10,16,17]. The individual unit of GNT structure consists of a uniform nanotwinned region with columnar grains containing preferentially (111)-oriented nanotwin lamellae. The characteristic size of a unit is defined by its thickness or volume fraction within a gradient period, while its key microstructural features are grain size and twin lamellae thickness. As the structural gradient defined as the slope of hardness along depth increases, gradient deformation becomes more heterogeneous, with GNDs increasingly forming as bundles of concentrated dislocations (BCDs) along the gradient [10,16]. These GNDs or BCDs generate substantial back stress, further enhancing both strength and work hardening. Strengthening is also amplified by optimizing gradient configurations, such as positioning hard layers at the surface and soft layers at the core, or by increasing the volume fraction of the transition region to broaden the GND-affected zone [17–19].

In addition to gradient design, the intrinsic work hardening capability of individual units is a critical factor in governing the mechanical response of GNS metallic material. Generally, high work hardening improves deformation stability and suppresses strain localization by promoting strong dislocation interactions [20]. Our previous work revealed that greater differences in work hardening between units enhance incompatibility at interfaces, thereby increasing GND accumulation and further improving strengthening [21].

In this study, we investigate the role of overall work hardening of units in governing the strengthening and deformation behavior of GNT Cu. To isolate this effect, three GNT Cu samples with a systematically increased overall work hardening capacity of units were designed, while maintaining constant gradient parameters, including structural gradient, gradient distribution and volume fraction of units. The enhancement in strengthening and work hardening is assessed relative to homogeneous nanotwinned (HNT) counterparts having matched average hardness. Through comparison of plastic strain gradient, post-deformation microstructures, and hardening responses, we elucidate the underlying mechanisms through which unit-level work hardening

* Corresponding authors.
E-mail addresses: zcheng13s@imr.ac.cn (Z. Cheng), llu@imr.ac.cn (L. Lu).
[1] Lei Lu was an Editor of the journal during the review period of the article. To avoid a conflict of interest, Lei Lu was blinded to the record and another editor processed this manuscript.

https://doi.org/10.1016/j.scriptamat.2025.116973
Received 7 July 2025; Received in revised form 26 August 2025; Accepted 30 August 2025
Available online 5 September 2025

influences the performance of GNT Cu.

Three representative GNT Cu samples were prepared via direct current electrodeposition, with a fixed current density of 30 mA/cm^2. The electrolyte temperature profile was changed to modulate unit-level work hardening. GNT-I was deposited by linearly heating the electrolyte from 15 to 30 °C over 8 h, followed by symmetric cooling to 15 °C. Additional parameters are detailed in Ref. [16]. GNT-II and GNT-III samples were fabricated using higher thermal cycles from 20 to 35 °C and 25 to 40 °C, respectively, maintaining the same heating and cooling rates as GNT-I. For comparison, free-standing homogeneous nanotwinned (HNT) Cu samples, named HNT-I, HNT-II and HNT-III, were synthesized at constant temperatures of 23, 27, and 32 °C, matching the average temperature of the corresponding GNT samples. All deposited HNT and GNT Cu samples had a thickness of ~400 μm.

Cross-sectional microstructures of GNT and HNT Cu samples, both before and after tensile testing, were examined using a FEI Nova NanoSEM 460 field emission gun scanning electron microscope (SEM) in backscattering electron imaging (BSE) mode. The height variation on lateral surfaces of GNT Cu samples were measured using confocal laser scanning microscopy (CLSM, Olympus LEXT OLS4100).

Depth-dependent hardness distributions were obtained using a Qness Q10 $A+$ microhardness tester under a 50 g load with a 10 s dwell time. Flat dog-bone shaped flat tensile specimens (gauge length of 5 mm and a width of 2 mm) were machined from the as-deposited electrodeposited GNT and HNT Cu foils via electric spark cutting and then polished mechanically and electrochemically. Uniaxial quasi-static tensile tests were performed on an Instron 68TM-5 microtester at a strain rate of 5×10^{-3} s^{-1} at ambient temperature. Strain was measured using a contactless MTS LX300 laser extensometer. A minimum of five specimens per condition were tested to ensure the statistical reliability.

SEM cross-sections (Fig. 1) confirm that all samples possess a characteristic nanotwinned structure, with nanoscale twin lamellae oriented perpendicular to the growth direction, embedded within micron-scale columnar grains, as seen in Ref. [22]. In GNT-I, the twin thickness increases from 21 (surface) to 51 nm (core), while grain size ranges from 2.0 to 7.6 μm. The corresponding cross-sectional hardness drops linearly from 1.7 to 1.1 GPa, yielding an average hardness of 1.4 GPa and the structural gradient (the slope of hardness along depth) of $s = 3$ GPa/mm (Fig. 1d1). GNT-II and GNT-III exhibit progressively wider ranges of grain size (2.7~16 μm and 5.4~20 μm, respectively) and twin thickness (27~76 nm and 37~84 nm, respectively). Their hardness spans decrease accordingly to 1.5~0.9 (GNT-II) and 1.3~0.7 GPa (GNT-III), with corresponding average hardness values of 1.2 and 1.0 GPa. Clearly, all GNT Cu samples share the same structural gradient slope, confirming that the only varied parameter is the microstructure span cross units, which determines their overall work hardening capacity.

Reference HNT Cu samples displayed homogeneous microstructures across all sections, as shown in SEM images in Fig. 1a2-c2. From HNT-I, -II to -III, the average grain size increases from 4.6 ± 0.3, 5.7 ± 0.3 to 7.5 ± 0.5 μm, and the average twin thickness increases from 30±2, 39 ±3, to 45±5 nm. Correspondingly, the average cross-sectional hardness decreases from 1.40±0.03, 1.25±0.04 to 1.05±0.03 GPa, comparable to values of GNT-I, -II and -III samples, respectively.

Fig. 2a shows the tensile engineering stress-strain curves of GNT Cu samples in comparison to their free-standing HNT counterparts. The average yield strength decreases from 416±10, 372±7 to 296±12 MPa from HNT-I, -II to -III samples while the uniform elongation is improved from 4.0, 9.1 to 12.1 %. GNT samples exhibit higher yield strength than their HNT counterparts, while uniform elongation is comparable or slightly reduced. These results indicate an obvious extra strengthening effect induced by GNT structures.

Fig. 2b presents the variation of work-hardening rates ($\Theta = d\sigma/d\varepsilon$) of all samples as a function of true strain. Two typical stages are observed: the elastic-plastic transition stage with a steep decrease of work hardening rate before the strain of ~3 %, and the steady plastic deformation stage where work hardening reduces slowly at larger strains.

To evaluate the work hardening capacity, we defined Θ_c to account for strain by integrating the work-hardening rate over the true strain during the steady-state deformation stage. The inset in Fig. 2b shows the Θ_c increases from 11.2 to 43.7 MPa in HNT-I to -III, indicating the enhanced unit-level hardening capacity from GNT-I to -III.

GNT-I to -III display additional work hardening beyond that of HNT-I

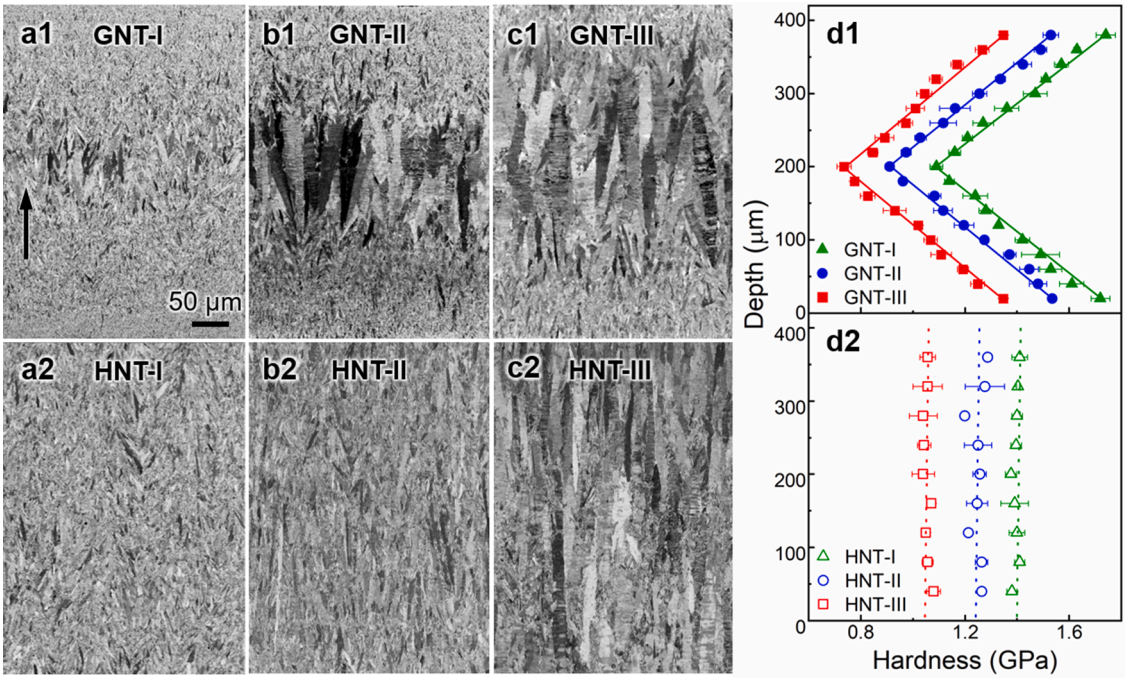

Fig. 1. Cross-sectional SEM image of gradient nanotwinned (GNT) Cu samples: GNT-I (a1), GNT-II (b1) and GNT-III (c1), and their corresponding homogeneous nanotwinned (HNT) counterparts: HNT-I (a2), HNT-II (b2) and HNT-III (c2). The cross-sectional hardness distributions along the depth direction for GNT (d1) and HNT Cu samples (d2), as indicated.

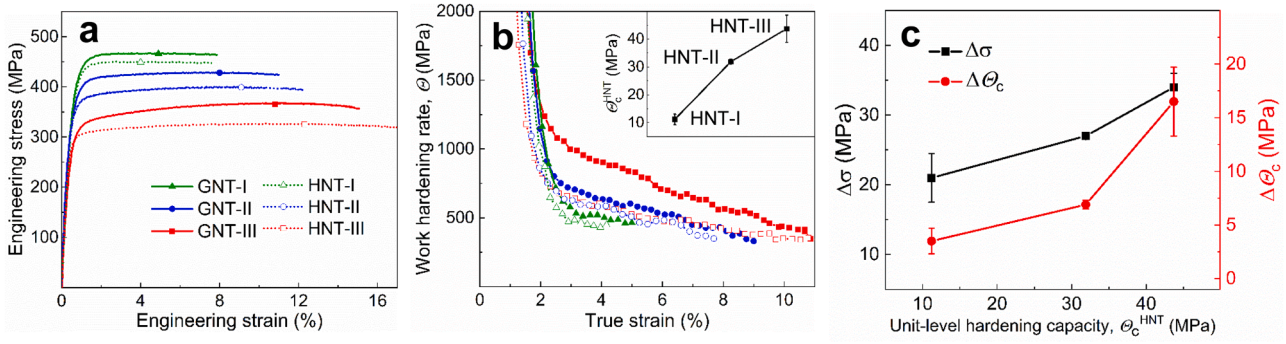

Fig. 2. Engineering tensile stress-strain curves (a) and work hardening rate (Θ) vs. true strain curves (b) of GNT Cu in comparison to HNT Cu. The inset of (b) shows work hardening capacity (Θ_c^{HNT}) of HNT Cu. The extra strengthening (Δσ) and extra work hardening capacity ($\Delta\Theta_c$) with unit-level hardening capacity (Θ_c^{HNT}) of GNT Cu(c).

to -III. At the elastic-plastic transition stage, all GNT Cu samples exhibit higher work hardening rates compared to their HNT counterparts. During the steady deformation stage, GNT-I shows a slightly higher work hardening rate than HNT-I, while GNT-II demonstrates a significantly enhanced work hardening rate relative to HNT-II, indicating the presence of additional work hardening. This effect is further amplified in GNT-III.

The extra strengthening and work hardening capacity can be quan-

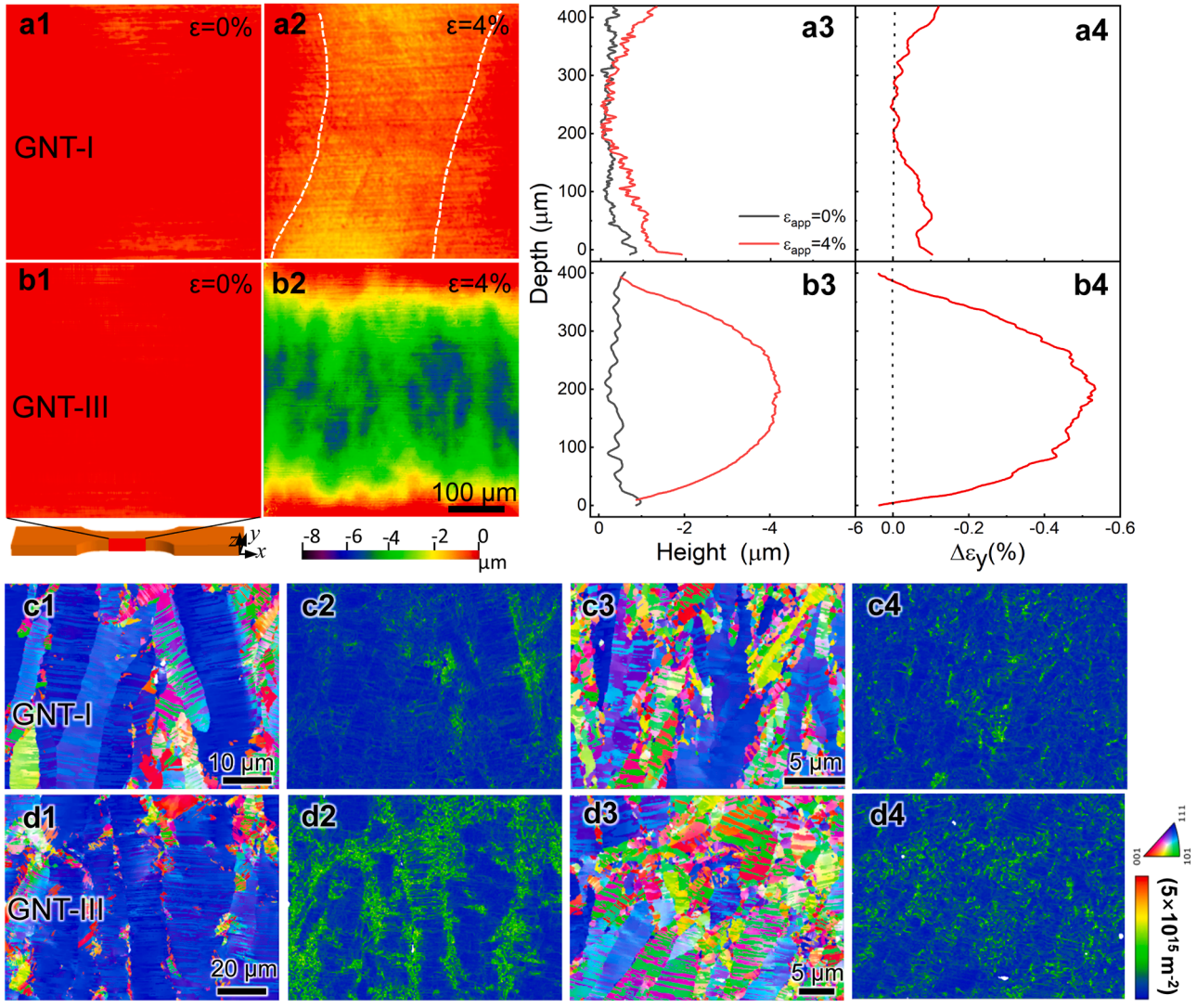

Fig. 3. Height profiles of the lateral surface and corresponding relative lateral strain in GNT-I and GNT-III samples. (a1, a2) The height contour maps of the lateral surface of GNT-I at $\varepsilon = 0$ and 4 %, respectively. The strain localization region is outlined by two white lines in (a2). Average height profile (a3) and average relative lateral strain $\Delta\varepsilon_y$ (a4) for GNT-I. (b1-b4) show the corresponding data for GNT-III, in the same format as (a1-a4). Cross-sectional EBSD images (c1, c3) and dislocation density mappings (c2, d4) of the core (c1, c2) and near-surface regions (c3, c4) of fractured GNT-I. (d1-d4) are same as (c1-c4) and except for fractured GNT-III.

titatively estimated by $\Delta\sigma = \sigma_{GNT} - \sigma_{HNT}$ and $\Delta\Theta_c = \Theta_c^{GNT} - \Theta_c^{HNT}$, respectively, where σ_{GNT} and σ_{HNT} are yield strength of GNT Cu and their HNT counterparts, respectively, and $\Theta_c^{GNT}$and Θ_c^{HNT} are their respective work hardening capacities at the steady-state deformation stage. As shown in Fig. 2c, both extra strengthening and work hardening capacity increase from 21 to 34 MPa, and from 3.5 to 16.5 MPa, respectively, from GNT-I to III, correlating with increasing overall work hardening of units.

The characterization of gradient strain in GNT samples provides critical insights into the intrinsic deformation mechanisms. As illustrated in Fig. 3a, the height profile across the lateral surface (x-z plane) was measured to calculate the distribution of the relative lateral strain $\Delta\varepsilon_y$ in GNT Cu. The lateral surface of the as-prepared GNT-I sample appears nearly flat, with minor variations due to mechanical polishing, as shown in Fig. 3a1. However, after tensile deformation at $\varepsilon = 4$ % (Fig. 3a2), the height of the central region (outlined by the white dashed line) decreases relative to the left and right sides, indicating strain localization along the tensile axis (x-axis).

By averaging the surface height along the tensile direction, the average height profile across the sample thickness (z-axis) is obtained (Fig. 3a3). Subtracting the post-deformation profile ($\varepsilon_{app} = 4$ %) from the pre-deformation profile yields the net height change, Δh. The distribution of relative lateral strain $\Delta\varepsilon_y$ is calculated as $\Delta\varepsilon_y = 2\Delta h/W_0$, where W_0 is the initial width of the tensile samples. As shown in Fig. 3a4, $|\Delta\varepsilon_y|$ at surface (hard unit) is notably greater than in the core (soft unit), indicating a strain discrepancy of approximately 0.1 % and a corresponding strain gradient of 2 m^{-1}.

The lateral surface height profile of deformed GNT-III (Fig. 3b1 and 3b2) exhibits pronounced variation along the thickness direction (y-axis), in contrast to the strain localization observed along the tensile axis in GNT-I. As illustrated in Fig. 3b3, the central region corresponding to the soft unit exhibits a substantially lower height compared to the hard units on both surfaces—opposite to the deformation pattern seen in GNT-I. This indicates that the soft unit undergoes greater shrinkage strain than the hard unit (Fig. 3b4). The discrepancy in $|\Delta\varepsilon_y|$ between hard and soft units reaches 0.53 %, and the corresponding strain gradient η_y increases to 27 m^{-1}, reflecting a significantly enhanced gradient deformation compared to GNT-I.

The deformation morphologies and dislocation storage of the GNT Cu are further compared by using EBSD in Fig. 3. The deformed GNT-I sample maintains a strong (111) texture across the soft core to hard surface units (Fig. 3c1 and 3c3). The corresponding GNDs mapping reveals that dislocations primarily accumulate at GBs, with fewer observed in grain interiors (Fig. 3c2 and 3c4). The overall GND densities is 7.3 × 10^{14} and 9.1 × 10^{14} m^{-2}in the soft core and hard surface units, respectively. In contrast, while deformed GNT-III exhibits a similar (111) texture, it generates a higher density of GNDs (Fig. 3d1-d4). Notably, substantial GNDs storage occurs within grain interiors, beyond just the GB. The overall GND density reaches 12.8 × 10^{14} and 9.3 × 10^{14} m^{-2} in the soft and hard units of GNT-III, respectively, both of which are higher than their counterparts in GNT-I. These results align with the observed strain gradient evolution in both samples (Fig. 3a1-b4), confirming that an enhanced unit-level work hardening capacity promotes greater GND storage, leading to stronger strengthening and hardening.

To elucidate the underlying deformation mechanisms, we analyzed the microstructures of deformed GNT Cu samples. Fig. 4 compares the microstructures near the tensile fracture region of GNT-I and GNT-III, where the true strain $\varepsilon_T \approx 33$ % was estimated based on cross-section shrinkage. In GNT-I, the soft core unit exhibits grain boundary (GBs)-dominated plastic deformation. Fragmented nanotwins at GBs (highlighted by yellow arrows in Fig. 4a1) suggest the accumulation and pile-up of threading dislocations along TBs, similar to observations in HNT Cu [22]. Several prominent shear bands, characterized by fragmented nanotwins and extending across multiple grains, are also observed. These shear bands are oriented at approximately 30°∼45° relative to the tensile axis, consistent with the maximum shear direction typically seen in nanostructured metals. Notably, more shear bands are observed in the surface (hard unit) than in the core (soft unit) (Fig. 4a2).

In contrast, GNT-III exhibits multiple elongated BCDs via the accumulation of GNDs, which comprise two types of dislocations: a minority of Mode I dislocations with both glide plane and glide direction inclined to twin boundaries (TBs) and a majority of Mode II dislocations with glide plane inclined and glide direction parallel to TBs, respectively, by systemically dual-beam TEM diffraction analysis in previous studies [10, 16,17]. In the hard unit (Fig. 4b2), several BCDs are observed as regions of strong contrast (indicated by red arrows) within the interiors of columnar grain aligned along the gradient direction. Notably, these remain intact and unfragmented, in contrast to the GB degradation observed in GNT-I. These BCDs have an average width of approximately 0.5 μm, consistent with previously reported GNT Cu samples [16]. In the soft unit, the BCDs become slightly coarser, with an average width of 1.9 μm (Fig. 4b1).

We further compared the hardening behavior across the cross-

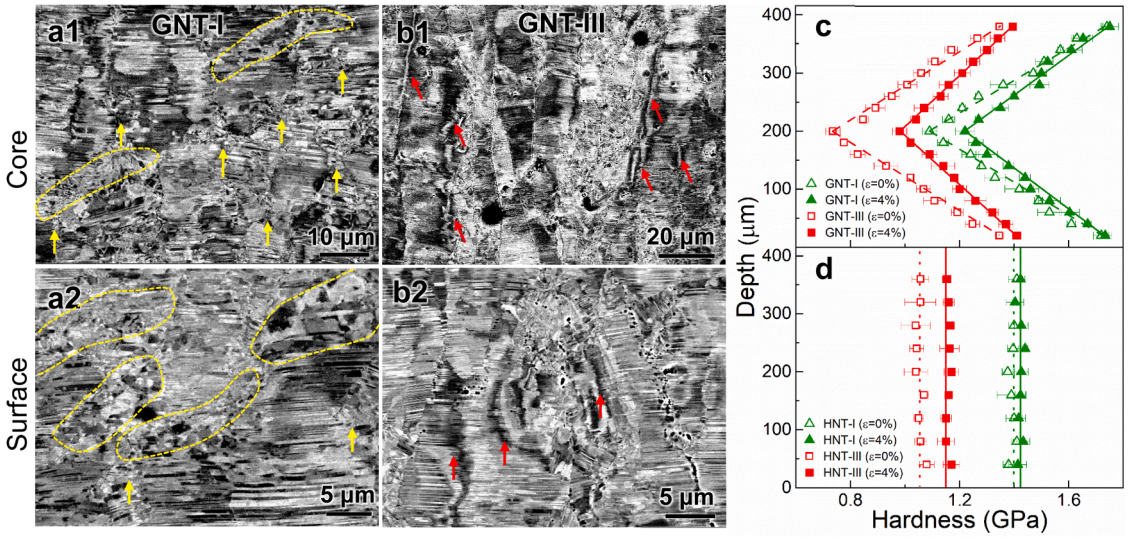

Fig. 4. Cross-sectional SEM images of the core (a1, b1) and near-surface regions (a2, b2) of fractured GNT-I (a1, a2) and GNT-III (b1, b2). Shear bands are outlined with dashed lines in (a1) and (a2). Twin fragments at grain boundaries and BCDs are marked by yellow and red arrows, respectively. (c) Hardness distribution across GNT-I and GNT-III at $\varepsilon = 0$ % and 4 %, compared to (d) HNT-I and HNT-III under the same strains levels.

sections of GNT-I and GNT-III. For GNT-I (Fig. 4c), the surface hardness after deformation remains nearly unchanged compared to the initial state, indicating the negligible hardening. The hardening increment, ΔH, is defined as $\Delta H = H - H_0$, where H and H_0 represent the hardness after and before tensile deformation, respectively. Toward the core region, the hardening increases noticeably, up to approximately 11.9 %, resulting in an average hardening of 5.2 % across all sections, comparable to that observed in HNT-I (Fig. 4d). In contrast, GNT-III exhibits a consistently higher post-deformation hardness cross all units compared to the initial stage. The hardening is substantially enhanced, increasing from 4.2 % at the surface to 33.2 % in the core. The average hardening reaches 14.9 %, exceeding that of HNT-III (10.0 %), which indicates the presence of significant extra hardening in GNT-III.

The hardening of structural units in GNT Cu arises from two mechanisms. First, intrinsic hardening is determined by microstructural characteristics, where larger grain size and twin thickness result in greater strength. Consequently, intrinsic hardening increases from surface to core in each GNT Cu sample. More importantly, an additional hardening component is generated by the storage of GNDs, which scales with the magnitude of the strain gradient. Notably, the strain gradient in GNT-III is significantly larger than in GNT-I, resulting into superior extra hardening throughout all sections of the former. This enhancement originates from improved unit-level work-hardening capacity, which suppresses strain localization and there amplifies the strain gradient. In other essence, the high unit-level work hardening is critical prerequisite for gradient deformation and the resulting extra hardening.

By integrating the above experiment results, we conclusively demonstrate that enhancing the overall work hardening capacity of individual units leads to simultaneous increases in both extra strengthening and work hardening in GNT Cu. Higher work hardening promotes the development of a more pronounced strain gradient, which drives the accumulation of GNDs, resulting in substantial additional hardening. In contrast, lower work hardening suppresses the strain gradient and exacerbates strain localization, thereby limiting the potential for extra hardening.

The strain gradient plays a critical role in strengthening gradient nanostructured metals to achieve superior mechanical properties. According to classical strain gradient plasticity theory [23–25], strain gradients induce the formation of GNDs, with GND density directly proportional to the magnitude of the strain gradient. These GNDs generate strong kinematic hardening or long-range back stresses on other mobile dislocations, which not only enhance dislocation resistance (contributing to higher strength) but also intensify forest dislocation interactions, thereby boosting work hardening capacity [22,26–28].

Typically, strain gradients are attributed to the built-in gradient structures that undergo a progressively yielding process. In gradient-structured metals, such as GNT Cu, the soft unit yields first due to its lower yield strength, while the hard unit yields later. As a result, plastic strain progressively decreases from the soft to the hard unit, producing an internal strain gradient - even under uniform total strain during tensile deformation [10,16,19]. This implies that the strain gradient is governed by the yield strength gradient, or more broadly, by the structural gradient across the cross-section of GNT Cu or other GNS metals [5,16,29].

We find that the strain gradient of GNT Cu is significantly influenced by the overall work hardening capacity of its units, even when the structural gradient remains constant. The strain localization induced by the lower unit-level work hardening enable GNT-I distinct gradient deformation mechanism and the smaller strain gradient opposite to GNT-III, as further discussed in the below.

In GNT-I, limited work hardening capacity promotes strain localization over uniform plastic flow during tensile deformation. This behavior originates from an ultrafine grain size, which restricts the available space for dislocation storage [30] and promotes shear bands, the primary deformation mechanism often observed in brittle metals under extreme conditions [31]. Furthermore, the smaller grain size intensifies this strain localization, resulting into plastic strain to increase from the core to surface and forming the observed gradient. Crucially, this strain localization induces a plastic strain gradient opposite to in direction to that generated by progressive yielding, thereby diminishing the overall strain gradient (Fig. 3a4).

In contrast, the superior work hardening capacity of the structural units in GNT-III suppresses strain localization and promotes uniform plastic deformation. This provides the necessary condition for the development of a strain gradient induced by progressively yielding induced strain gradient. As a result, a large number of GNDs form and self-organize into BCDs throughout all units. These BCDs not only generate long-range back stress that contributes to extra strengthening but also mitigate dislocation annihilation at GBs, thereby sustaining extra work hardening.

Furthermore, the extra strengthening can be enhanced by increasing the strength disparity between units or the structural gradient [16,21,32]. This intensifies gradient deformation and promotes the storage of more GNDs. The magnitude of strain gradient and thus the extra strengthening are also governed by the spatial distribution of structural units. Key factors include their volume fractions, the thickness of gradient layers between them, and the gradient order [17,33–35]. Strategic modulation of these parameters can collectively maximize the extra strengthening effects, enabling superior mechanical properties in GNS metals.

In summary, the overall work hardening capacity of individual units is revealed as a critical factor governing gradient deformation and the resulting extra strengthening/hardening effect in GNT Cu, even when the structural gradient remains constant. Higher unit work hardening suppresses strain localization and enables the formation of strain gradients driven by progressive yielding along the built-in structural gradient. Consequently, more GNDs are stored and organized into forming BCDs, which contribute to enhanced extra strengthening and work hardening. This finding not only advances the mechanistic understanding of gradient deformation, but also provides a new strategy for designing high-performance GNS metallic materials.

CRediT authorship contribution statement

Linhai Liu: Writing – original draft, Investigation, Formal analysis, Data curation. **Che Liu:** Formal analysis. **Jin Zheng:** Formal analysis. **Zhao Cheng:** Writing – review & editing, Formal analysis. **Lei Lu:** Writing – review & editing, Conceptualization.

Declaration of competing interest

The authors declare that they have no known competing financial interests or personal relationships that could have appeared to influence the work reported in this paper.

The author is an Editorial Board Member/Editor-in-Chief/Associate Editor/Guest Editor for this journal and was not involved in the editorial review or the decision to publish this article.

Acknowledgements

We acknowledge financial support from the National Natural Science Foundation of China (NSFC), Grant No 92163202, 92463302, U24A2027, 52422102 & 52371124), the Global Common Challenges Project (Grant No 172GJHZ2023075GC), the Youth Innovation Promotion Association, Chinese Academy of Sciences (CAS), and the National Key R&D Program of China (Grant No 2024YFA1210601 and 2024YFA1210602).

References

[1] X.Y. Li, L. Lu, J.G. Li, X. Zhang, H.J. Gao, Mechanical properties and deformation mechanisms of gradient nanostructured metals and alloys, Nat. Rev. Mater. 5 (9) (2020) 706–723.

[2] Y.T. Zhu, X.L. Wu, Heterostructured materials, Prog. Mater. Sci. 131 (2023) 101019.

[3] B. Xu, H. Duan, X. Chen, J. Wang, Y. Ma, P. Jiang, F. Yuan, Y. Wang, Y. Ren, K. Du, Y. Wei, X. Wu, Harnessing instability for work hardening in multi-principal element alloys, Nat. Mater. 23 (6) (2024) 755–761.

[4] C.X. Huang, Y.F. Wang, X.L. Ma, S. Yin, H.W. Höppel, M. Göken, X.L. Wu, H.J. Gao, Y.T. Zhu, Interface affected zone for optimal strength and ductility in heterogeneous laminate, Mater. Today 21 (7) (2018) 713–719.

[5] Y.F. Wang, C.X. Huang, M.S. Wang, Y.S. Li, Y.T. Zhu, Quantifying the synergetic strengthening in gradient material, Scr. Mater. 150 (2018) 22–25.

[6] J. Wang, Z. Qing, S. Shuai, A. Misra, Strength and plasticity of nanolaminated materials, Mater. Res. Lett. 5 (1) (2017) 1–19.

[7] A. Misra, J.P. Hirth, R.G. Hoagland, Length-scale-dependent deformation mechanisms in incoherent metallic multilayered composites, Acta Mater. 53 (18) (2005) 4817–4824.

[8] Z. Zeng, X.Y. Li, D.S. Xu, L. Lu, H.J. Gao, T. Zhu, Gradient plasticity in gradient nano-grained metals, Extreme Mech. Lett. 8 (2016) 213–219.

[9] H.J. Gao, Y. Huang, W.D. Nix, J.W. Hutchinson, Mechanism-based strain gradient plasticity— I. Theory, J. Mech. Phys. Solids. 47 (6) (1999) 1239–1263.

[10] Z. Cheng, L.F. Bu, Y. Zhang, H.A. Wu, T. Zhu, H.J. Gao, L. Lu, Unraveling the origin of extra strengthening in gradient nanotwinned metals, Proc. Natl. Acad. Sci. u S. a 119 (3) (2022) e2116808119.

[11] L.P. Kubin, A. Mortensen, Geometrically necessary dislocations and strain-gradient plasticity: a few critical issues, Scr. Mater. 48 (2) (2003) 119–125.

[12] H.J. Gao, Y.G. Huang, Geometrically necessary dislocation and size-dependent plasticity, Scr. Mater. 48 (2) (2003) 113–118.

[13] L. Bardella, A deformation theory of strain gradient crystal plasticity that accounts for geometrically necessary dislocations, J. Mech. Phys. Solids. 54 (1) (2006) 128–160.

[14] H. Mughrabi, Dual role of deformation-induced geometrically necessary dislocations with respect to lattice plane misorientations and/or long-range internal stresses, Acta Mater. 54 (13) (2006) 3417–3427.

[15] H. Mughrabi, Deformation-induced long-range internal stresses and lattice plane misorientations and the role of geometrically necessary dislocations, Philos. Mag. 86 (25–26) (2006) 4037–4054.

[16] Z. Cheng, H.F. Zhou, Q.H. Lu, H.J. Gao, L. Lu, Extra strengthening and work hardening in gradient nanotwinned metals, Science (1979) 362 (6414) (2018) 559.

[17] Z. Cheng, T. Wan, L.F. Bu, L. Lu, Effect of volume fractions of gradient transition layer on mechanical behaviors of nanotwinned Cu, Acta Mater. 242 (2023) 118456.

[18] Y. Kim, Z. Cheng, G.H. Gu, L. Lu, H.S. Kim, Mechanical behavior of gradient nanotwinned Cu: a dislocation-based constitutive model incorporating gradient effects, Mater. Sci. Eng. A 925 (2025) 147805.

[19] Y. Zhang, Z. Cheng, T. Zhu, L. Lu, Mechanics of gradient nanostructured metals, J. Mech. Phys. Solids. 189 (2024) 105719.

[20] J. Wang, A. Misra, Strain hardening in nanolayered thin films, Curr. Opin. Solid State Mat. Sci. 18 (1) (2014) 19–28.

[21] T. Wan, Z. Cheng, L.F. Bu, L. Lu, Work hardening discrepancy designing to strengthening gradient nanotwinned Cu, Scr. Mater. 201 (2021) 113975.

[22] Z.S. You, L. Lu, K. Lu, Tensile behavior of columnar grained Cu with preferentially oriented nanoscale twins, Acta Mater. 59 (18) (2011) 6927–6937.

[23] M.F. Ashby, The deformation of plastically non-homogeneous materials, Philos. Mag. 21 (170) (1970) 399–424.

[24] W.D. Nix, H.J. Gao, Indentation size effects in crystalline materials: a law for strain gradient plasticity, J. Mech. Phys. Solids. 46 (3) (1998) 411–425.

[25] N.A. Fleck, M.F. Ashby, J.W. Hutchinson, The role of geometrically necessary dislocations in giving material strengthening, Scr. Mater. 48 (2) (2003) 179–183.

[26] M.A. Meyers, A. Mishra, D.J. Benson, Mechanical properties of nanocrystalline materials, Prog. Mater. Sci. 51 (4) (2006) 427–556.

[27] C.J. Bayley, W.A.M. Brekelmans, M.G.D. Geers, A comparison of dislocation induced back stress formulations in strain gradient crystal plasticity, Int. J. Solids. Struct. 43 (24) (2006) 7268–7286.

[28] Y. Zhang, Z. Cheng, L. Lu, T. Zhu, Strain gradient plasticity in gradient structured metals, J. Mech. Phys. Solids. 140 (2020) 103946.

[29] J.J. Li, G.J. Weng, S.H. Chen, X.L. Wu, On strain hardening mechanism in gradient nanostructures, Int. J. Plast. 88 (2017) 89–107.

[30] T.J. Rupert, D.S. Gianola, Y. Gan, K.J. Hemker, Experimental observations of stress-driven grain boundary migration, Science (1979) 326 (5960) (2009) 1686–1690.

[31] C.S. Hong, N.R. Tao, X. Huang, K. Lu, Nucleation and thickening of shear bands in nano-scale twin/matrix lamellae of a Cu–Al alloy processed by dynamic plastic deformation, Acta Mater. 58 (8) (2010) 3103–3116.

[32] X.C. Lu, Y.L. Xu, H. Ran, G.H. Fan, S. Gao, N. Tsuji, C.X. Huang, H.J. Gao, Y. W. Zhang, The role of layer strength ratio in enhancing strain hardening and achieving strength-ductility synergy in heterostructured materials, Acta Mater. 289 (2025) 120928.

[33] Z. Cheng, L.F. Bu, Y. Zhang, H.A. Wu, T. Zhu, L. Lu, Characterization of gradient plastic deformation in gradient nanotwinned Cu, Acta Mater. 246 (2023) 118673.

[34] Z. Cheng, T. Wan, L. Lu, Interface strain gradient enabled high strength and hardening in laminated nanotwinned Cu, Acta Mater. 256 (2023) 119138.

[35] Z. Cheng, L. Lu, The effect of gradient order on mechanical behaviors of gradient nanotwinned Cu, Scr. Mater. 164 (2019) 130–134.